Distinct superconducting states in the pressure-induced metallic structures of the nominal semimetal Bi_{4}Te_{3}

J. R. Jeffries, A. L. Lima Sharma, P. A. Sharma, C. D. Spataru, S. K. McCall, J. D. Sugar, S. T. Weir, and Y. K. Vohra

Phys. Rev. B **84**, 092505 — Published 27 September 2011

DOI: 10.1103/PhysRevB.84.092505

Distinct superconducting states in the pressure-induced metallic structures of the nominal semimetal Bi_4Te_3

J. R. Jeffries,[1] A. L. Lima Sharma,[2,3] P. A. Sharma,[2] C. D. Spataru,[2]
S. K. McCall,[1] J. D. Sugar,[2] S. T. Weir,[1] and Y. K. Vohra[4]

[1] *Condensed Matter and Materials Division, Lawrence Livermore National Laboratory, Livermore, CA 94550, USA*
[2] *Materials Physics Department, Sandia National Laboratory, Livermore, CA 94551, USA*
[3] *Department of Physics and Astronomy, San Jose State University, San Jose, CA 95192, USA*
[4] *Department of Physics, University of Alabama at Birmingham, Birmingham, Alabama 35294, USA*

The end members, Bi and Bi_2Te_3, of the infinitely adaptive $(Bi_2)_m(Bi_2Te_3)_n$ series of compounds have not only been revealed to be topological insulators under the appropriate conditions, but have also been shown to be superconductors under pressure, suggesting the potential for bulk superconductor-topological-insulator interfaces and associated quantum computing applications. Herein, we report the pressure-dependent evolution of the structure and electrical transport of the nominal semimetal Bi_4Te_3, a member of the $(Bi_2)_m(Bi_2Te_3)_n$ series. Under pressure, Bi_4Te_3 undergoes several structural phase transformations, ultimately yielding a metallic body-centered-cubic structure exhibiting superconductivity with a maximum T_c=8.4 K at 16.2 GPa. The occurrence of structure-dependent superconductivity in Bi_4Te_3 is remarkably similar to the end members of the $(Bi_2)_m(Bi_2Te_3)_n$ series, intimating a convergence to high-pressure universal behavior that may expose the subtle variations that lead to the topological insulating and superconducting states in these systems.

PACS numbers: 64.30.Jk, 74.70.Ad, 74.62.Fj
Keywords: structural transformations, superconductivity, magnetotransport

Recently, superconductor-topological-insulator junctions have been predicted to induce Majorana bound states and the tantalizing prospects for quantum computing [1–3]. While this proximity-induced effect might suffice for quantum computing, the realization of bulk superconductivity in $Cu_xBi_2Se_3$ intimates a more controllable route to superconducting-topological-insulator interfaces [4–6]. Furthermore, the observation of superconductivity under pressure in Bi_2Te_3 suggests the general feasibility of tuning between topological insulating and superconducting states within the same system [7].

The nominal semimetal Bi_4Te_3 is a member of the trigonal, infinitely adaptive $(Bi_2)_m(Bi_2Te_3)_n$ series, which is composed of Bi and Te planes assembled from alternating layers of Bi_2 and Bi_2Te_3 building blocks [8]. The end members of this series, Bi and Bi_2Te_3, both display topological insulating behavior, the former through alloying with Sb [9–11]. With applied pressure, Bi and Bi_2Te_3 exhibit several different crystal structures [12–14] and distinct superconducting states [7, 15–17]. The relationships between these high-pressure superconducting states and the ambient-pressure topologically insulating states are important components to our understanding of the conditions favoring these states. The $(Bi_2)_m(Bi_2Te_3)_n$ family provides an extensive series that may help to illuminate the subtle differences that create topologically insulating or superconducting states.

Herein, we report a comprehensive structural and electrical transport characterization of semimetal Bi_4Te_3 under pressure using diamond anvil cells (DAC). High-pressure x-ray diffraction reveals several structural transformations, culminating in the stabilization of a body-centered-cubic structure at the highest pressures measured. Accompanying these structural changes are modifications in the electronic structure, which manifest a shift from semimetallic behavior at ambient pressure to metallic behavior in the high-pressure phases. Finally, two distinct superconducting states are observed, with the highest-pressure superconducting state exhibiting a maximum critical temperature comparable to those of Bi and Bi_2Te_3 at elevated pressures.

Stoichiometric amounts of elemental Bi and Te (99.99%, Alfa Aesar) were combined in an evacuated quartz tube and melted at 700 °C for 5 days. The melt was then quenched in liquid nitrogen and subsequently annealed at 440 °C for 14 days. X-ray diffraction and electron microscopy confirmed that the samples were single phase Bi_4Te_3 ($R\bar{3}m$) with large ($\sim$1 mm) grains. For electrical transport measurements under pressure, single crystal grains were harvested and loaded into an eight-probe designer DAC [18, 19] with steatite as the pressure-transmitting medium and ruby as the pressure calibrant [20, 21]. Electrical transport measurements were performed as a function of temperature and magnetic field using the AC Transport option in a Quantum Design PPMS. For structural studies, a conventional DAC was loaded with powdered Bi_4Te_3, fine Cu powder (3-6 μm, Alfa Aesar) as the pressure calibrant, and neon as a pressure-transmitting medium. Room-temperature, angle-dispersive x-ray diffraction experiments were performed at the HPCAT beamline (16 BM-D) of the Advanced Photon Source at Argonne National Laboratory. A 5x5 μm, 30 keV (λ_{inc}=0.4134 Å) incident x-ray beam, calibrated with CeO_2, was used. 2D diffraction pat-

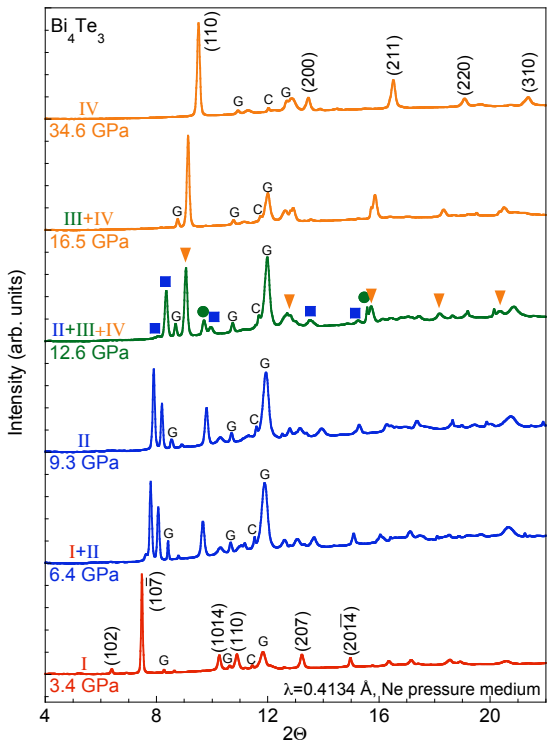

FIG. 1: (color online). Selected x-ray diffraction patterns of Bi_4Te_3 under pressure revealing the different structures: Bi_4Te_3-I ($R\bar{3}m$), Bi_4Te_3-II ($C2/m$), Bi_4Te_3-III, and Bi_4Te_3-IV ($Im\bar{3}m$). Diffraction peaks from the copper pressure marker and gasket are denoted by a "C" and "G," respectively. Some of the prominent Bragg reflections from the Bi_4Te_3-I and Bi_4Te_3-IV structures are labeled. The pronounced peaks in the multiphase diffraction data at 12.6 GPa are assigned to their respective phases: blue squares-Bi_4Te_3-II; green circles-Bi_4Te_3-III; orange triangles-Bi_4Te_3-IV.

terns were collected with a Mar345 image plate, collapsed to 1D intensity versus 2Θ plots using the program FIT2D[22], and refined using the programs EXPGUI [23, 24] and Jade. *Ab initio* calculations were performed using the Quantum Espresso package [25] employing the density functional theory (DFT) formalism with a local density approximation for the exchange correlation potential and including spin-orbit effects [26].

At ambient pressure, Bi_4Te_3 crystallizes in the trigonal $R\bar{3}m$ space group with a=4.451 Å and c=41.888 Å (3 formula units per unit cell). Under pressure, the $R\bar{3}m$ crystal structure compresses relatively easily (bulk modulus B_0≈52 GPa). Near 6.4 GPa, a structural phase transformation occurs (Fig. 1), yielding a slightly stiffer (B_0≈77 GPa) monoclinic unit cell with lattice parameters a=4.3110(34), b=4.6052(38), and c=6.2641(38) Å with β=110.22°. The reflections from Bi_4Te_3-II index well to a $C2/m$ space group, yielding a unit cell volume of 116.70 Å^3. Presuming that pressure drives the system into a structure with a lower atomic volume, the unit cell of Bi_4Te_3-II should be constructed from no fewer than 4 atoms; 4- and 5-atom unit cells would imply volume collapses of approximately 3 and 22%, respectively, for the I-II phase transition. We conservatively propose that Bi_4Te_3-II undergoes a moderate volume collapse, suggesting that it is composed of 4 atoms per unit cell. The $C2/m$ space group and the number of atoms per unit cell for Bi_4Te_3 are then identical to those of the high-pressure Bi-II phase [27]. With only 4 atoms per unit cell, Bi_4Te_3-II has fewer than one formula unit per unit cell. In order to maintain the 4:3 Bi:Te ratio in Bi_4Te_3-II, Bi and Te atoms must reside with stoichiometric occupancy at equivalent atomic positions within the unit cell of Bi_4Te_3-II.

Near 11.5 GPa, another phase transformation occurs, producing a multiphase sample where Bi_4Te_3-II coexists with Bi_4Te_3-III and Bi_4Te_3-IV. This multiphase system persists up to approximately 16.5 GPa. Because of its coexistence with other phases, indexing Bi_4Te_3-III was not possible. Bi_4Te_3-IV, on the other hand, appears as a single phase for pressures in excess of 16.5 GPa and is easily indexed to a body-centered-cubic (*bcc*) $Im\bar{3}m$ unit cell with a=3.6702(2) Å and a volume of 49.44 Å^3 (B_0≈120 GPa). With two atoms per unit cell, the bcc Bi_4Te_3-IV phase, like that of Bi_4Te_3-II, contains fewer than one formula unit per unit cell and thus must be described with a similar stoichiometric occupancy of the atomic positions. The high-pressure Bi_4Te_3-IV phase is effectively a disordered bcc alloy of Bi and Te, identical to the high-pressure structures of Bi-V and Bi_2Te_3-IV [12, 14].

Low-temperature $\rho(T)$ data (Fig. 2a) reveal the onset of superconductivity at 8.2 GPa with a T_c=2.1 K. With further pressure, T_c increases slightly followed by a discontinuous increase in the transition temperature near 13 GPa. At P_c=16.2 GPa, the superconducting transition temperature reaches a maximum T_c=8.4 K, very close to the observed maximum T_c of Bi (8.4 K) and Bi_2Te_3 (9.4 K) under pressure [15–17]. For pressures above 16.2 GPa, the superconducting transition width sharpens, hovering near a width of about 1 K, and T_c decreases monotonically down to T_c=4.1 K at 42.5 GPa.

Magnetotransport measurements (Fig. 2b) conducted at 10 K show a clear change in the Hall resistivity (ρ_{xy}) as a function of pressure. At ambient pressure, Bi_4Te_3 is best described as a semimetal due to signatures of ambipolar conduction in Hall effect, Seebeck, and Nernst measurements [28]. While low carrier mobility precludes a quantitative analysis of the ambient-pressure magnetotransport, the presence of electron and hole bands is strongly implied by the qualitative shape of $\rho_{xy}(H)$. At 8.2 GPa, the sign of ρ_{xy} became negative, but the nonlinear field dependence of ρ_{xy} clearly remains, implying that multiband effects still play a role at this pressure. This multiband behavior yields above 17.8 GPa to a linear field dependence with a minimum slope near 19.7

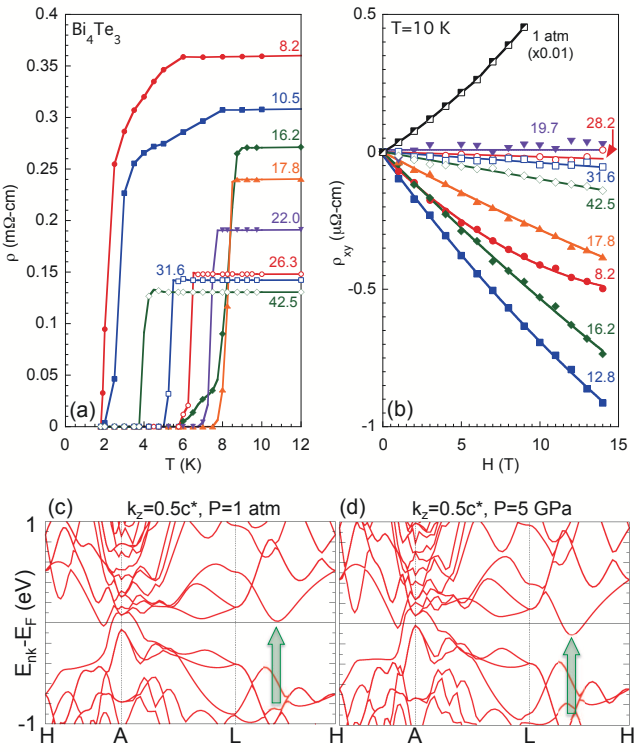

FIG. 2: (color online) (a) Low-temperature electrical resistivity $\rho(T)$ for various pressures (in GPa, denoted by text near each curve) revealing the onset and development of superconductivity. (b) $\rho_{xy}(H)$ for various pressures. (c) LDA band structure calculations confirm the ambient-pressure semimetallic behavior of Bi_4Te_3 and (d) reveal the pressure-dependent appearance of an electron-like pocket between the L and H points (green arrows).

GPa. At 8.2 GPa, the low-field slope of ρ_{xy} implies a carrier concentration of order 10^{21} cm^{-3}—a borderline value between the expectations for a metal and a semimetal or degenerate semiconductor—while at 31.6 GPa, the ρ_{xy} data suggest a carrier concentration of order 10^{23} cm^{-3}—closer to that of a typical metal.

In order to illuminate the multiband transport in Bi_4Te_3, band structure calculations were performed. These calculations have been restricted to the ambient-pressure ($R\bar{3}m$) phase, because solutions for the site-disordered, high-pressure phases II and IV are intractable with the *ab initio* DFT routine utilized. Figures 2c and d show the electronic dispersions along certain high-symmetry directions in the hexagonal Brillouin zone with k_z=0.5$c^\star$ ($c^\star$ is the reciprocal lattice vector perpendicular to the Bi/Te layers). At ambient pressure (Fig. 2c), a small hole-like section of Fermi surface is visible at zone center (A), a small electron pocket crosses the Fermi level in the A-H direction near zone center, and another electron pocket dips near the Fermi level between the L and H points. This calculation supports the conclusion that both holes and electrons contribute to transport at ambient pressure, but also indicates that any realistic transport model should account for more than two bands. At 5 GPa (Fig. 2d), the zone-center hole band increases in size, the small electron pocket near zone center remains nearly unaltered, and the electron pocket between the L and H points crosses the Fermi level. Applied pressure thus causes large electron-like pockets to appear near the zone edges of the Fermi surface. The persistence of the zone-center hole pocket and the appearance of these large electron pockets under pressure explain the persistent multiband behavior as well as the change in sign of ρ_{xy}.

The pressure-dependent evolution of the structure and electrical transport of Bi_4Te_3 are summarized in Fig. 3. Near 6 GPa, Bi_4Te_3 transforms from its ambient pressure, $R\bar{3}m$ structure into a monoclinic $C2/m$ structure similar to elemental Bi [12]. Concomitant with this structural transformation is the reduction in the value of ρ(10 K) and a change in the sign of the Hall coefficient, R_H. Superconductivity develops out of this Bi_4Te_3-II phase, but with a relatively low critical temperature of T_c=2.1 K at 8.2 GPa. Increasing pressure compresses the monoclinic structure, which exhibits only a slightly stiffer lattice than the Bi_4Te_3-I phase. With the lattice compression from 6 to 12 GPa, superconductivity is enhanced, reaching T_c=3.7 K at 12.8 GPa.

Applying further pressure instigates the ingrowth of the *bcc* phase of Bi_4Te_3-IV, which manifests a new superconducting state with a T_c greater than twice that of the maximum T_c observed in the Bi_4Te_3-II phase. With increasing pressure, Bi_4Te_3 transforms completely to the *bcc* phase and $|R_H|$ reaches a minimum, indicating a high-carrier-density metallic phase. T_c reaches a maximum value of 8.4 K at 16.2 GPa. Pressures above 20 GPa result in an increase in $|R_H|$—corresponding to a decrease in the carrier concentration—and a simultaneous suppression of T_c. The simultaneous occurrence of a high-carrier-density metal and a maximum in T_c upon entering into a *bcc* crystal structure is also evident in Bi and Bi_2Te_3 [15, 17]. Indeed, the pressure-dependent evolution of T_c in the *bcc* phases of Bi_4Te_3, Bi_2Te_3, and Bi are strikingly similar (inset Fig. 3c).

In summary, Bi_4Te_3 displays two distinct superconducting states arising from different high-pressure structural modifications: monoclinic Bi_4Te_3-II, a low-carrier-density multiband metal; and *bcc* Bi_4Te_3-IV, which displays archetypal metallic behavior. The striking similarities between the pressure-dependent structures and evolutions of T_c in the *bcc* phases of Bi, Bi_2Te_3, and Bi_4Te_3 hint at universal behavior manifesting under pressure within the $(Bi_2)_m(Bi_2Te_3)_n$ series. Understanding how the disparate ambient-pressure states of the $(Bi_2)_m(Bi_2Te_3)_n$ series ultimately converge to this universal high-pressure behavior could provide insights into the conditions favoring topological insulators and super-

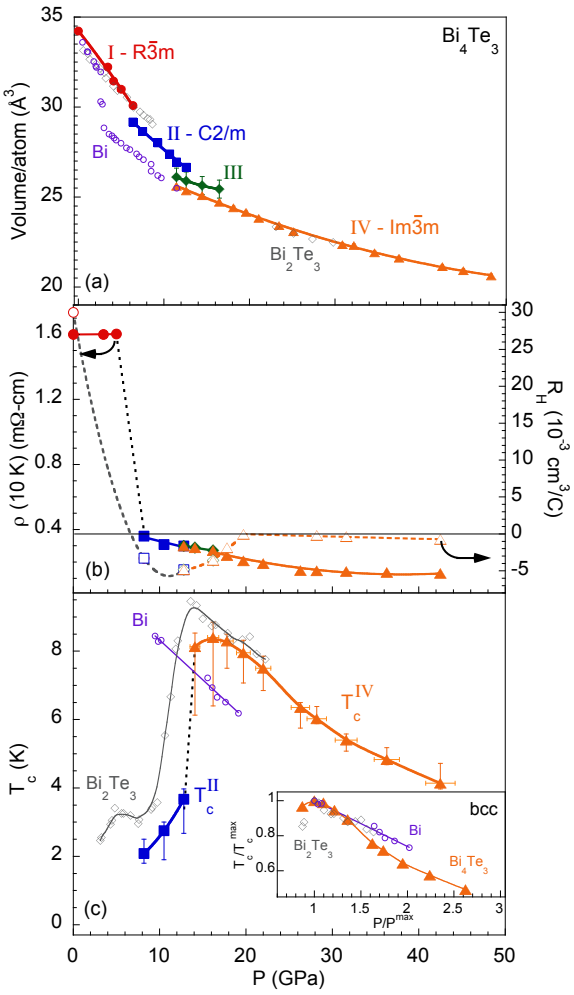

FIG. 3: (color online). Pressure-dependent evolution of the structural and electronic properties of Bi_4Te_3. (a) The equation of state (volume/atom) of Bi_4Te_3 reveals three pressure-induced structural transformations; data for Bi [12] (open, purple circles) and Bi_2Te_3 [14] (open, grey diamonds) are included. (b) The electrical resistivity at 10 K, ρ (10 K) (closed symbols, left axis) and the Hall coefficient, R_H, (open symbols, right axis) suggest metallization under pressure. (c) The evolution of superconductivity under pressure reveals a maximum T_c =8.4 K near 16.2 GPa, within the bcc phase. Vertical error bars represent widths of the superconducting transitions, while horizontal error bars represent uncertainty in pressure. Data for Bi [15] and Bi_2Te_3 [17] under pressure are included (open symbols) for comparison. Inset: scaled evolution of T_c/T_c^{max} versus P/P^{max} in the bcc phases of Bi_4Te_3, Bi_2Te_3, and Bi. In all cases, solid and dashed lines are guides to the eye.

conductors.

We thank K. Visbeck, J. Park-Klepeis, and C. Kenny-Benson for assistance and beamline support. Portions of this work were performed under LDRD. Lawrence Livermore National Laboratory is operated by Lawrence Livermore National Security, LLC, for the U.S. Department of Energy (DOE), National Nuclear Security Administration (NNSA) under Contract DE-AC52-07NA27344. Portions of this work were performed at HPCAT (Sector 16), Advanced Photon Source (APS), Argonne National Laboratory. HPCAT is supported by CIW, CDAC, UNLV and LLNL through funding from DOE-NNSA, DOE-BES and NSF. Use of the APS, an Office of Science User Facility operated for the U.S. DOE Office of Science by Argonne National Laboratory, was supported by the U.S. DOE under Contract No. DE-AC02-06CH11357. Beamtime was provided through the General User Proposal program. Sandia is a multiprogram laboratory operated by Sandia Corporation, a Lockheed Martin Company, for the U.S. DOE NNSA under Contract No. DE-AC04-94AL85000. Work at Sandia was supported by the LDRD program. Y. K. V. acknowledges support from DOE-NNSA Grant No. DE-FG52-10NA29660.

[1] L. Fu and C. L. Kane, Phys. Rev. Lett. **100**, 096407 (2008)
[2] J. D. Sau, *et al.*, Phys. Rev. B **82**, 094522 (2010).
[3] L. Hao and T. K. Lee, Phys. Rev. B **83**, 134516 (2011).
[4] X. -L. Qi, *et al.*, Phys. Rev. Lett. **102**, 187001 (2009).
[5] Y. S. Hor, *et al.*, Phys. Rev. Lett. **104**, 057001 (2010).
[6] L. Fu and E. Berg, Phys. Rev. Lett. **105**, 097001 (2010).
[7] J. L. Zhang, *et al.*, Proc. Natl. Acad. Sci. **108**, 24 (2011).
[8] J. W. G. Bos, *et al.*, Phys. Rev. B **75**, 195203 (2007).
[9] D. Hsieh, *et al.*, Science **323**, 919 (2009).
[10] P. Roushan, *et al.*, Nature **460**, 1106 (2009).
[11] Y. L. Chen, *et al.*, Science **325**, 178 (2009).
[12] O. Degtyareva, M. I. McMahon, and R. J. Nelmes, High Press. Res. **24**, 319 (2004).
[13] A. Nakayama, *et al.*, High Press. Res. **29**, 245 (2009).
[14] M. Einaga, *et al.*, Phys. Rev. B **83**, 092102 (2011).
[15] M. A. Il'ina and E. S. Itskevich, Sov. Phys.-JETP Lett. **11**, 218 (1970).
[16] M. A. Il'ina and E. S. Itskevich, Sov. Phys.-Solid State **13**, 2098 (1972); **17**, 154 (1975).
[17] C. Zhang, *et al.*, Phys. Rev. B **83**, 140504(R) (2011).
[18] S. T. Weir, *et al.*, Appl. Phys. Lett. **77**, 3400 (2000).
[19] D. D. Jackson, *et al.*, Phys. Rev. B **74**, 174401 (2006).
[20] H. K. Mao, J. Xu, and P. M. Bell, J. Geophys. Res. **91**, 4673 (1986).
[21] W. L. Vos and J. A. Schouten, J. Appl. Phys. **69**, 6744 (1991).
[22] A. Hammersley, *et al.*, High Press. Res. **14**, 235 (1996).
[23] A. C. Larson and R. B. Von Dreele, Los Alamos National Laboratory Report LAUR 86-748 (1994).
[24] B. H. Toby, J. Appl. Crystallogr. **34**, 210 (2001).
[25] P. Giannozzi, *et al.*, http://www.quantum-espresso.org
[26] W. Kohn and L. J. Sham, Phys. Rev. **140**, A1133 (1965).
[27] R. M. Brugger, R. B. Bennion, and T. G. Walton, Phys. Lett. A **24**, 714 (1967).
[28] See Supplementary Material at [URL] for a description of the semimetal behavior of Bi_4Te_3 under ambient conditions.